Noninvasive, in vivo imaging of the mouse brain using photoacoustic microscopy

Erich W. Stein, Konstantin Maslov, and Lihong V. Wang

Citation: Journal of Applied Physics **105**, 102027 (2009); doi: 10.1063/1.3116134
View online: http://dx.doi.org/10.1063/1.3116134
View Table of Contents: http://scitation.aip.org/content/aip/journal/jap/105/10?ver=pdfcov
Published by the AIP Publishing

Noninvasive, *in vivo* imaging of the mouse brain using photoacoustic microscopy

Erich W. Stein, Konstantin Maslov, and Lihong V. Wang[a)]
Department of Biomedical Engineering, Optical Imaging Laboratory, Washington University in St. Louis, Campus Box 1097, One Brooking Drive, St. Louis, Missouri 63130, USA

(Received 25 April 2008; accepted 12 July 2008; published online 19 May 2009)

Noninvasive, high resolution imaging of mouse brain activity is poised to provide clinically translatable insights into human neurological disease progression. Toward noninvasive imaging of brain activity through the hemodynamic response, the dark-field photoacoustic microscopy (PAM) technique was enhanced to image the cortex vasculature of the mouse brain *in vivo* using endogenous hemoglobin contrast. Specifically, the PAM system was redesigned to efficiently collect photoacoustic waves originating from cortical vessels, providing high (70 μm lateral and 54 μm axial) resolution images of the mouse brain vasculature with a contrast-to-noise ratio of 25 dB. These findings confirm the efficacy of PAM to noninvasively image vascular structures in the mouse brain and the potential to image mouse brain function by tracking the hemodynamic response.
 [DOI: 10.1063/1.3116134]

I. INTRODUCTION

In recent years, genetically altered mouse models have been developed to mimic neurological diseases of humans. These animal models permit the controlled study of the cause, effect, and treatment of neurological diseases, and are poised to provide clinically translatable insights.[1] Hence, approaches to screen mouse brain function throughout disease progression are desired, making noninvasive techniques most appealing for longitudinal studies of the same subject. Since direct noninvasive techniques of locating and measuring brain activity (i.e., electrical signals) are not available, downstream surrogates for neuronal activity are used to noninvasively image brain activity. The most commonplace of which is the "hemodynamic response"—changes in blood oxygenation, volume, and flow of local brain regions induced by neuronal activity.[2]

The distinctive spectral characteristics of hemoglobin make optical imaging techniques a good choice to monitor the hemodynamic response with high sensitivity. However, to provide noninvasive images of brain activity with high spatial resolution, these techniques must overcome the effects of light scattering from the scalp and skull.[3] Photoacoustic (PA) imaging techniques are ideally suited for this application.[4] PA techniques use short pulses of laser irradiation to induce thermoelastic expansion of biological tissues, which subsequently produces wideband ultrasonic waves (PA waves) that can be detected with an ultrasound receiver. Because PA wave generation can be induced by absorption of diffuse photons and ultrasonic scattering in biological tissues is two orders of magnitude less than that of optical scattering, PA imaging techniques have been used to image structures deeper than one optical transport mean free path in tissue with a resolution in the tens of microns.[5] Furthermore, since PA waves arise from absorbed optical energy distributions within tissues, PA image contrast is directly related to optical absorption. With hemoglobin being one of the dominant absorbers in tissues, PA imaging techniques are well equipped to image hemoglobin concentration and oxygenation in vascular networks *in vivo* by using multiple optical wavelengths.[5]

Other techniques such as μPET, μSPECT, μCT, and fMRI have been successfully implemented to noninvasively image mouse brain structures *in vivo*. Functional brain imaging with μPET and μSPECT, however, require exogenous contrasts and exhibit inherently low resolution (millimeter scale).[6] fMRI is capable of imaging mouse brain structure and function by exploiting the endogenous differences in magnetic properties of oxy- and deoxyhemoglobin,[7] but is unable to distinguish between increased blood oxygenation or decreased blood volume.[3,8] PA tomography (PAT) was previously used to noninvasively image the cortex vasculature in the *in vivo* rat model and image neural activity by tracking local changes in cortical blood volume arising from somatosensory excitation;[9] however, PAT in this implementation exhibits poor depth resolution. Additionally, the aforementioned techniques are reconstruction based, requiring complete image acquisition to accurately measure single points of interest. Photoacoustic microscopy (PAM), however, operates in reflection mode and uses spherically focused ultrasonic detection to directly form images, affording direct measurements of regions of interest with notable depth and temporal resolution.[5,10]

Toward the goal of imaging brain activity in the mouse model, the PAM technique was enhanced to noninvasively image the cortical vasculature of the *in vivo* mouse brain in this work.[5,8] Specifically, we increased the image acquisition rate and modified the ultrasonic detector to decrease image artifacts caused by ultrasonic reflections from the skull.

[a)]Author to whom correspondence should be addressed. Tel.: 314-935-6152. FAX: 314-935-7448. Electronic mail: lhwang@biomed.wustl.edu.

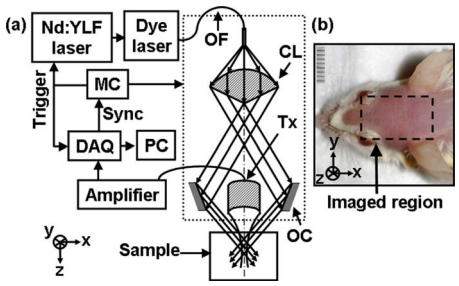

FIG. 1. (Color online) (a) System diagram. OF: optical fiber; CL: conical lens; Tx: transducer; OC: optical condenser; MC: motor controller. (b) Digital photograph of a prepared animal taken prior to imaging, depicting the 10×8 mm^2 scanned region.

II. SYSTEM DESCRIPTION

The key components of our system, shown in Fig. 1(a), are a kilohertz-pulse-repetition-rate tunable laser system, consisting of a wavelength tunable dye laser (Cobra, Sirah; Rhodamine 6G as the gain medium) pumped by a Nd:YLF laser (INNOSLAB, EdgeWave), a single element focused ultrasonic transducer, a mechanical scanning stage, and a data acquisition system. For a detailed description of system components and operating principles, readers are referred to previous work.[5,11] Briefly, laser output was coupled to an optical fiber, expanded through a conical lens and focused into the sample with an optical condenser. The resulting dark-field illumination pattern reduces optical fluence at the sample surface, partially averages superficial heterogeneities, and reduces superficial paraxial contributions.[10] In this system, maximum optical fluence at 570 nm was measured to be 12 mJ/cm^2, less than the American National Standards Institute (ANSI) safety limit for 400–700 nm (20 mJ/cm^2). Laser-induced PA waves were detected by a focused ultrasonic transducer confocal with the optical lens. Images were formed by converting the recorded time-resolved PA signals into a one-dimensional depth-resolved image ("A-lines") along the z-axis using the sound velocity in soft tissue (1.54 mm/μs). The rate of A-line acquisition is limited by the laser pulse repetition rate and mechanical scanning of the stage and was about 1 KHz for the PAM used in this work. By raster scanning across the xy plane, volumetric images of the sample were acquired.

III. ANIMAL PROCEDURES

Swiss Webster mice (Harlan Sprague Dawley Inc., ~25 g) were selected as the animal model in this study. All *in vivo* procedures were carried out in conformity with the guidelines of the National Institutes of Health and in compliance with the Washington University Institutional Animal Care and Use Committee (IACUC). The mouse was initially anesthetized using a cocktail (83 mg/kg ketamine and 17 mg/kg xylazine) administered by intraperitoneal injection. Body temperature was maintained at 37 °C with a temperature controlled heating pad. Prior to imaging, the hair on the scalp was removed with an over-the-counter depilatory cream (Nair), as shown in Fig. 1(b), and the animal was secured in a stereotaxic frame with a pair of ear pins and a tooth bar. Following hair removal and stereotaxic mounting, the anesthesia was transitioned to vaporized isoflurane (1.5 L/min O_2, 0.75% isoflurane) for the duration of all experimental procedures. After the completion of all experimental procedures, the animal was euthanized with a pentobarbital overdose administered via tail vein injection.

IV. RESULTS AND DISCUSSION

Using the setup previously described,[5,11] a 50 MHz ultrasonic detector (bandwidth: 70%; NA: 0.44; focal length: 6.7 mm; depth of focus: 0.3 mm) and 570 nm illumination was used to image the cortical vasculature by raster scanning over the region of interest shown in Fig. 1(b). However, a clear image of the cortical vasculature (~0.5 mm below the scalp surface) was not obtained, despite the ability to image structures 3 mm below the skin surface of the rat abdomen.[10] Since the acquisition of PAM images is predicated upon optical energy delivery to excite PA waves and the subsequent collection of those PA waves via ultrasound detection, difficulties in imaging the cortical vasculature could arise from poor optical energy delivery or low acoustic energy collection. With this in mind, Monte Carlo simulations[12] using reported tissue optical properties[13] were used to compare the optical fluence at the brain surface to the optical fluence at 3 mm below the abdominal skin surface. Simulation results reveal that the optical fluence at the brain surface is approximately 17 times greater than the optical fluence at 3 mm below the abdominal skin surface, implying that the optical energy delivered to the cortical vessels on the brain surface was sufficient to generate PA waves. These results suggest that challenges in imaging the cortical vasculature arise from difficulties in collecting transcranial PA waves, which could be due to the acoustic impedance mismatch between the skull and surrounding soft tissues, as well as the acoustic attenuation of PA waves propagating through the skull. The most critical being the acoustic impedance mismatch between the skull and surrounding tissues, which could cause the pressure waves generated from the scalp to be reflected from the skull and be detected at a similar time as those originating from the cortical vasculature, thereby occluding the PA footprint of the cortical vessels. Acoustic attenuation from the skull would curtail the PA waves generated from the cortical vessels, further complicating distinction. Correspondingly, experiments were conducted to examine how the skull affects the propagation of high frequency PA waves, with hopes of providing insight on optimizing the transcranial collection of PA waves generated from the brain vasculature.

Due to size limitations of the mouse skull, the parietal bone of a freshly harvested rat skull was used as a surrogate. The parietal bone was immersed in water between two coaxially oriented unfocused ultrasonic transducers with 6 mm apertures. Ultrasound transmission through the parietal bone was measured at various incident angles and normalized to the system frequency response (Fig. 2). When holding the frequency constant, these data show decreased ultrasound transmission until a local minimum at ~25° is observed. At incident angles above 25°, the transmission of acoustic waves through the skull increases with incident angle. A

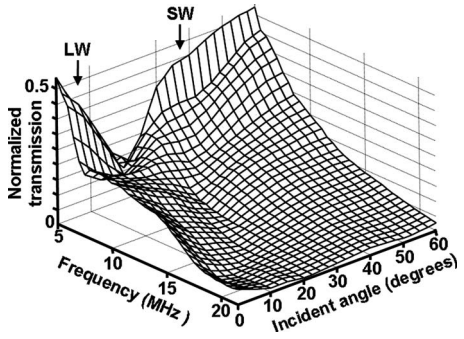

FIG. 2. (a) Transmission coefficient of ultrasound through the rat parietal bone vs ultrasonic frequency and incident angle. LW: predominantly longitudinal wave components; SW: converted shear wave components.

similar trend has been shown by others,[14] where incident acoustic waves beyond Snell's critical angle undergo a mode conversion from incident longitudinal waves to shear waves at the skull boundaries, then back into longitudinal waves at the interfacial layers (i.e., scalp or brain tissue). Additional calculations using known methods[15] and skull acoustic parameters inverted from transmission measurements revealed that the skull reflection coefficient decreased by a factor of 6 at the largest measured incident angle compared to normal incidence due to the similar acoustic impedances of shear waves in skull and soft tissue. Similar results were shown by others,[16] suggesting that the reflection of PA waves from the skull and the reverberations within the skull become less prominent at high incident angles. Thus, it may be possible to eliminate reverberations by using annular ultrasonic detection. The design feasibility of such a detector is currently under investigation in our laboratory. In this report, we used a high NA acoustic lens, which collects more PA wave energy at oblique incidence angles. High NA detection would also compensate for acoustic energy losses from skull transmission by collecting more PA wave energy at the expense of reducing the focal length and depth of focus.

According to the data shown in Fig. 2, a lower frequency bandwidth and larger aperture angle should allow more efficient collection of transcranial PA wave energy, leading to the design of an alternative detector for *in vivo* brain imaging. A 20 MHz central frequency transducer with 91% nominal bandwidth was selected, and an acoustic lens was machined into the silica delay line, yielding a NA of 0.64, a focal length of 5 mm. When compared to our previous detector (50 MHz, NA: 0.44), the 20 MHz transducer has a significant frequency overlap with the transcranial acoustic waves and a 14° increase in the acceptance half-angle [θ =arcsin(NA)], both of which should improve the collection efficiency of transcranial PA waves, according our results (Fig. 2).

Since the resolving power of the PAM used in this work is related to the ultrasonic detection properties, namely, bandwidth and NA, the lateral and axial resolutions were recharacterized using the 20 MHz transducer prior to *in vivo* imaging. Specifically, the lateral resolution and depth of focus are determined by the ultrasonic transducer sensitivity to a point pressure source, similar in principle to those of pure optical imaging systems.[17] The transducer sensitivity distribution can be approximated by the amplitude distribution in a converging spherical wave diffracted at a circular aperture.[17] The axial resolution, however, is determined by the ability to resolve PA transients in the time domain and is inversely proportional to the transducer bandwidth.[5] The lateral resolution was estimated by analyzing the PAM line spread functions [LSF, Fig. 3(a)] obtained by imaging a 6-μm-diameter carbon fiber [oriented along y, Fig. 1(a)] within the ultrasonic focal zone. The lateral resolution was experimentally determined to be 70 μm by taking the full width at half maximum (FWHM) of the lateral LSF, shown in Fig. 3(a). Our experimental data are similar to the estimated FWHM lateral resolution $r=0.72\lambda_0/\mathrm{NA}=80$ μm at the center wavelength, $\lambda_0=v_s/f_0=71$ μm, where v_s is the approximate sound velocity in soft tissue (1.5 mm/μs) and f_0 is the center frequency (21 MHz) of the received PA signal.

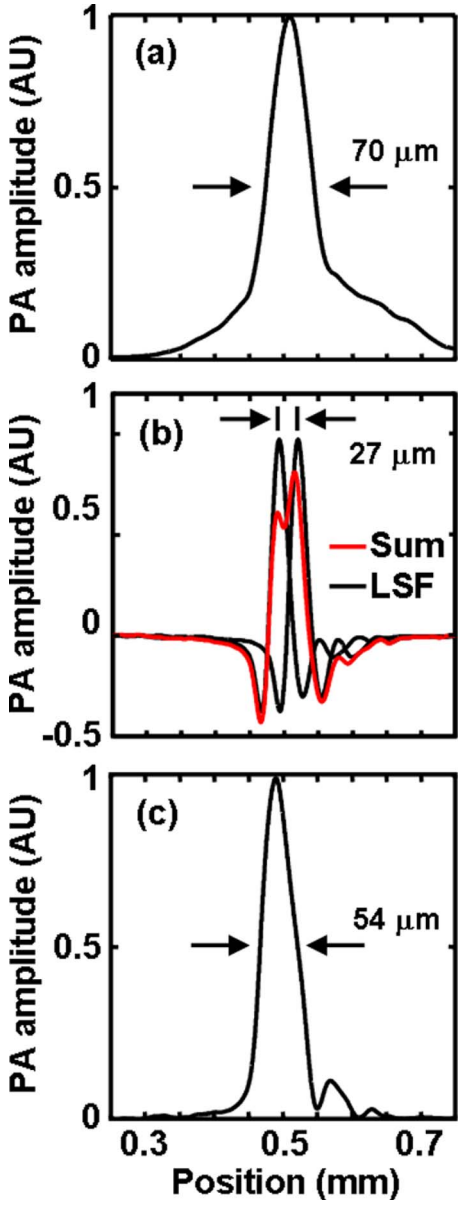

FIG. 3. (Color online) Spatial resolution of the 20 MHz PAM system. (a) Lateral LSF. (b) Shift-and-sum of the nonenveloped axial LSF. (c) Enveloped axial LSF. LSFs obtained by imaging a 6-μm-diameter carbon fiber in optically transparent media.

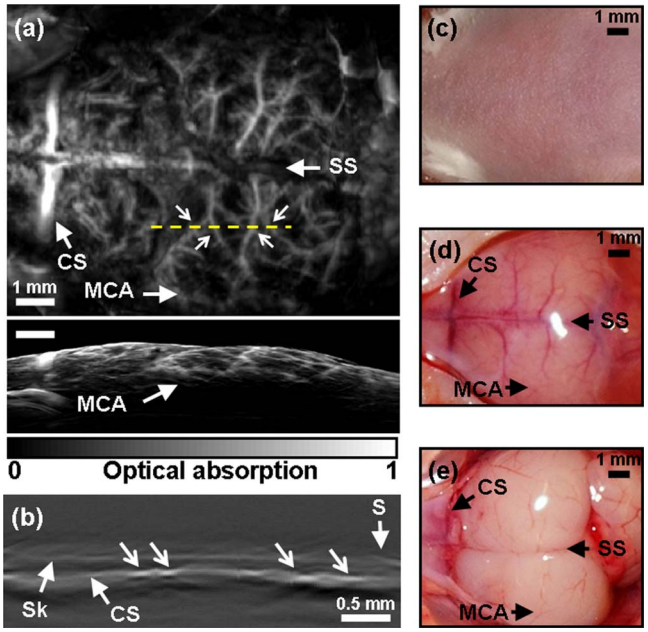

FIG. 4. (Color online) (a) Noninvasive *in vivo* PAM image of the mouse cortex vasculature (10×8 mm^2). SS: sagittal sinus; MCA: middle cerebral artery; CS: coronal suture. (b) B Scan denoting depth profile along dotted shown line in *a*. Arrow heads depict cortex vessels viewed in cross section. S: skin surface; Sk: skull; CS: brain cortex surface. (c) Photograph taken prior to imaging, when the cortex vessels are invisible to the naked eye. (d) Photograph taken after image acquisition and scalp removal. (e) Photograph taken after image acquisition and skull removal, showing an unobstructed view of the cortex vessels.

Previously, the axial resolution of our original 50 MHz system was estimated to be 15 μm by using the shift-and-sum of the nonenveloped axial LSF.[10] This method is based on the superposition of signals from two adjacent targets in a linear imaging system. Using the shift-and-sum of the nonenveloped axial LSF, the axial resolution of the 20 MHz system was determined to be 27 μm at a 10% contrast [Fig. 3(b)], demonstrating the scalability of the axial resolution with detector bandwidth. Here, we also present a more conservative estimate of the axial resolution by taking the FWHM of the enveloped axial LSF [Fig. 3(c)], yielding an axial resolution of 54 μm. The enveloped axial LSF was obtained by taking the absolute value of the Hilbert transformed raw PA signal. The theoretical axial resolution estimated with $v_s/\Delta f$ is 67 μm, where Δf is the FWHM (22 MHz) of the received PA signal frequency spectrum. These resolution values —70 μm lateral and 54 μm axial—represent the ideal case; in *in vivo* situations, the resolution degrades owing to the frequency dependence of ultrasound absorption in skull, which shifts the central frequency of the received PA signal from the central frequency of the ultrasonic transducer to ~12 MHz.

The estimated depth of focus $\Delta z=2\lambda_0/\mathrm{NA}^2$ was 400 μm.[17] Previous work characterized the resolution degradation of objects as a function of distance from the transducer focus in our PAM system.[18] Off-line processing, namely, a synthetic aperture focusing technique (SAFT), was used to "expand" the depth of focus. In this work, however, the structures of interests (major cortex vessels) are organized in a planar fashion on the cortex surface and were easily imaged within the transducer focal zone. Thus, out-of-focus resolution degradation was of little concern in this work, and SAFT was not employed.

Using the 20 MHz ultrasonic transducer and 570 nm illumination, PAM was used to noninvasively image the cortical vasculature of a mouse *in vivo*, by raster scanning over the region of interest [Fig. 1(b)]. A clear image of the cortical vasculature was obtained with the scalp and skull intact [Figs. 4(a) and 4(c)] in 7 min with step sizes of 20 and 40 μm along x and y, respectively. The maximum and mean contrast-to-noise ratio, defined as the intensity variation between the cortical vasculature and the background divided by the standard deviation of the background intensity, was 35 and 25 ±2 dB, respectively. Signal gating was used to remove the PA signals originating from the scalp, producing the axial and sagittal projections displayed in Fig. 4(a). Major vascular landmarks [sagittal sinus, middle cerebral artery, and coronal suture, Fig. 4(a)] were clearly identified and agree well with *in situ* anatomical photographs taken after image acquisition [Figs. 4(d) and 4(e)]. Furthermore, we emphasize a unique aspect of time-resolved PA imaging techniques: the ability to obtain two-dimensional depth resolved images by line scanning. These images, often denoted as "B-scans," can be acquired in less than 1 s (acquisition time is currently limited by mechanical scanning) and also allow depth-dependent tissues such as the skin surface, skull, brain cortex surface, and cortical vasculature to be clearly resolved [Fig. 4(b)]. Finally, while the 20 MHz detector used in this work was engineered to image major vessels on the brain surface, we were successfully able to image an obliquely embedded black anodized pin 3.2 mm below the scalp surface.

V. CONCLUSION

In summary, the acoustic transmission properties through the rodent skull were used to engineer a high frequency ultrasonic transducer capable of efficiently collecting PA waves originating from cortical vessels. This 20 MHz transducer (NA: 0.64) was successfully used to noninvasively image the cortical vasculature of the *in vivo* mouse brain, setting the stage for future work using PAM to noninvasively monitor small animal brain activity via the hemodynamic response.

ACKNOWLEDGMENTS

This work was sponsored by NIH Grant Nos. R01 EB000712 and R01 NS46214.

[1]M. Hafezparast, A. Ahmad-Annuar, N. W. Wood, S. J. Tabrizi, and E. M. Fisher, Lancet Neurol. **1**, 215 (2002).
[2]A. Grinvald, E. Lieke, R. D. Frostig, C. D. Gilbert, and T. N. Wiesel, Nature (London) **324**, 361 (1986).
[3]E. M. C. Hillman, J. Biomed. Opt. **12**, 051402 (2007).
[4]M. H. Xu and L. V. Wang, Rev. Sci. Instrum. **77**, 041101 (2006).
[5]H. F. Zhang, K. Maslov, G. Stoica, and L. V. Wang, Nat. Biotechnol. **24**, 848 (2006).
[6]R. S. Balaban and V. A. Hampshire, ILAR J. **42**, 248 (2001).
[7]G. Nair and T. Q. Duong, Magn. Reson. Med. **52**, 430 (2004).
[8]E. T. Ahrens and D. J. Dubowitz, NMR Biomed. **14**, 318 (2001).
[9]X. D. Wang, Y. J. Pang, G. Ku, X. Y. Xie, G. Stoica, and L. H. V. Wang, Nat. Biotechnol. **21**, 803 (2003).
[10]K. Maslov, G. Stoica, and L. V. Wang, Opt. Lett. **30**, 625 (2005).

[11]H. F. Zhang, K. Maslov, and L. V. Wang, Nat. Protocols **2**, 797 (2007).
[12]L. V. Wang, S. L. Jacques, and L. Zheng, Comput. Methods Programs Biomed. **47**, 131 (1995).
[13]V. Tuchin, *Tissue Optics: Light Scattering Methods and Instruments for Medical Diagnosis*, 2nd ed. (SPIE, Bellingham, WA, 2007).
[14]G. T. Clement, P. J. White, and K. Hynynen, J. Acoust. Soc. Am. **115**, 1356 (2004).
[15]C. L. Yapura, V. K. Kinra, and K. Maslov, J. Acoust. Soc. Am. **115**, 57 (2004); K. Maslov, R. Y. Kim, V. K. Kinra, and N. J. Pagano, Compos. Sci. Technol. **60**, 2185 (2000).
[16]P. J. White, G. T. Clement, and K. Hynynen, Ultrasound Med. Biol. **32**, 1085 (2006).
[17]M. Born and E. Wolf, *Principles of Optics*, Sixth ed. (Pergamon Press, Cambridge, 2006).
[18]M. L. Li, H. F. Zhang, K. Maslov, G. Stoica, and L. H. V. Wang, Opt. Lett. **31**, 474 (2006).